International Journal of Offshore and Polar Engineering (ISSN 1053-5381)

Vol. 33, No. 4, December 2023, pp. 367–379; https://doi.org/10.17736/ijope.2023.mm29

http://www.isope.org/publications

Physics-based Data-informed Prediction of Vertical, Catenary, and Stepped Riser Vortex-induced Vibrations

Andreas P. Mentzelopoulos, José del Águila Ferrandis, Samuel Rudy, Themistoklis Sapsis* and Michael S. Triantafyllou*, Department of Mechanical Engineering
Massachusetts Institute of Technology, Cambridge, Massachusetts, USA

Dixia Fan
School of Engineering, Westlake University
Hangzhou, Zhejiang, China

Semi-empirical models serve as current state-of-the-art prediction technologies for vortex-induced vibrations (VIV). Accurate prediction of the flexible body's structural response relies heavily on the accuracy of the acquired hydrodynamic coefficient database. The construction of systematic databases from rigid cylinder forced vibration experiments not only requires an extensive amount of time and resources but also is a virtually impossible task, given the wide multidimensional space the databases span. In this work, we improve the flexible cylinder VIV prediction by machine learning the hydrodynamic databases using measurements along the structure; such a methodology has been proven effective for vertical flexible risers in uniform and sheared flows using vibration amplitude and frequency data. This work demonstrates the effectiveness of the framework on flexible vertical risers in a stepped current and flexible catenary risers (with the catenary plane parallel or at an oblique angle with respect to the incoming flow). Moreover, the framework is applied to stepped (two-diameter) risers undergoing dual-frequency vibrations. Last, but not least, the framework is extended to using only sparse strain sensing. The predicted VIV responses using the learned hydrodynamic coefficient databases are compared with experimental observations.

INTRODUCTION

Observations of vortex-induced vibrations (VIV) date back thousands of years, first noticed by the ancient Greeks as "Aeolian tones"—sounds created by vortex-induced pressure fluctuations created by the wind passing around slender obstacles with a bluff cross section. Later, such vortices were sketched by Leonardo da Vinci. In recent years, following the development of bluff-shaped underwater equipment such as risers and cables, extensive studies have been conducted (Williamson et al., 2004, 2008; Bearman, 2011; Wu et al., 2012; Wang et al., 2020) on the subject, mainly to suppress VIV because of their destructive capabilities (Bernitsas et al., 2008; Baek and Karniadakis, 2009; Park et al., 2016). VIV affect bluff bodies in the presence of currents as a result of periodic shedding vortices developed in the wake aft bodies. The vortices lead to an alternating pressure variation that synchronizes with body motion, creating consistent vibrations that can cause extensive fatigue damage; however, they may also be exploited to harness clean and sustainable marine renewable energy (Bernitsas et al., 2019; N Li et al., 2022). Given the bluff nature of many modern offshore engineering equipment, such as cables, mooring lines, and marine risers (Fan and Triantafyllou, 2017; Wu et al., 2017; Fan, Wu, et al., 2019), a thorough understanding of the underlying physics of VIV is essential in controlling their effects, be they fatigue damage to offshore equipment or energy harnessed from flows (Bernitsas et al., 2008; Ma, Resvanis, and Vandiver, 2022).

VIV occur across a wide range of oscillating frequencies (Govardhan et al., 2002) known as the "lock-in" range, in which synchronization between vortex shedding and body motion takes place (Williamson and Govardhan, 2004; Wang et al., 2020). During lock-in, vibrations are typically self-limited to about one diameter. In addition, the vortex shedding frequency can differ from the Strouhal frequency of a fixed cylinder because the relative motion between the vibrating cylinder and the shed vortices significantly alters the effective fluid added mass (Wang, Fan, and Triantafyllou, 2021), resulting in a variable natural frequency as a function of stream velocity (Williamson, 1996).

Both experimental (Hover et al., 2001; Raghavan and Bernitsas, 2011; Xu et al., 2013; Resvanis et al., 2015; Resvanis and Vandiver, 2017, 2022) and numerical (Evangelinos et al., 2000; Wu et al., 2014, 2020; Kharazmi, Fan, et al., 2021; Meng et al., 2021; Wang, Fan, et al., 2021; Ma, 2022; Mentzelopoulos et al., 2022) studies demonstrate that significant variations of the fluid forces occur on an oscillating rigid cylinder as the incoming flow stream velocity and the cylinder motions change. Moreover, literature suggests that these variations are caused by changes in the vortex shedding pattern (Gopalkrishnan, 1993; Sarpkaya, 1995; Fan, Wang, et al., 2019). However, not only do the fluid forces depend heavily on the vortex shedding pattern; so do the hydrodynamic coefficients. Specifically, the added mass and lift coefficients may vary significantly as the vortex shedding pattern changes with both coefficients assuming positive and negative values.

Rigid cylinder-forced vibration experiments were the first attempts to estimate the hydrodynamic coefficients of oscillating cylinders undergoing VIV. The obtained coefficients were later

*ISOPE Member.

Received June 27, 2022; updated and further revised manuscript received by the editors January 20, 2023. The original version (prior to the final updated and revised manuscript) was presented at the Thirty-second International Ocean and Polar Engineering Conference (ISOPE-2022), Shanghai, China (virtual), June 5–10, 2022.

KEY WORDS: Vortex-induced vibrations, VIV, marine/SCR riser, hydrodynamic coefficient database, reduced-order modelling, data-informed modelling, sparse sensing.

used to predict rigid body VIV motions (Wang et al., 2003) and now serve as hydrodynamic coefficient databases used to estimate the fluid forces in semiempirical flexible riser VIV prediction codes (Triantafyllou et al., 1999; Larsen et al., 2001; Roveri et al., 2001; Zheng et al., 2011; Passano et al., 2016).

VIV of flexible bodies are significantly more complex than VIV of rigid bodies. Studies have been conducted to investigate the flow structure interaction of flexible bodies undergoing VIV and revealed very complex behaviors, including various structural modes, responses of traveling waves, and recently, multimodal and multifrequency vibrations (A Li et al., 2022). Insights on the flow past the bodies' wakes, in which boundary layers, shear layers, vortices, and the bodies themselves interact, have been revealed (Han et al., 2018; Fan, Jodin, et al., 2019; Kharazmi, Wang, et al., 2021; Wang, Li, et al., 2021; Ma, Lin, et al., 2022).

Semi-empirical models and prediction programs serve as the current state-of-the-art technologies for VIV prediction. One fundamental assumption these semiempirical models employ is strip theory. Among several other parameters, accurately estimating the hydrodynamic coefficients, such as the added mass coefficient C_{my} and the lift coefficient in phase with velocity C_{lv}, is key to the accurate prediction of the body's response (Yin et al., 2021). Estimating the coefficients is nontrivial and requires a large number of forced-vibration experiments with rigid cylinders using traditional methods (Gopalkrishnan, 1993). In addition, using systematic experiments to obtain a general hydrodynamic database suitable for various risers in various flow conditions is an impossible task.

In this work, we apply and extend a new paradigm (Rudy et al., 2022) of the hydrodynamic database inference directly from the observed response of flexible cylinders: an optimal parametric hydrodynamic database obtained from the comparison between experimental and VIVA (Triantafyllou et al., 1999; Zheng et al., 2011) prediction results.

MATERIALS AND METHODS

Modelling Flexible Body Vortex-induced Vibrations

The slender flexible body is modelled as a beam with varying material and geometric properties oscillating under the excitation of a hydrodynamic force (Triantafyllou et al., 1999; Zheng et al., 2011). The equation of motion is as follows:

$$m\frac{\partial^2 y}{\partial t^2} + b\frac{\partial y}{\partial t} - \frac{\partial}{\partial z}\left(T\frac{\partial y}{\partial z}\right) + \frac{\partial^2}{\partial z^2}\left(EI\frac{\partial^2 y}{\partial z^2}\right) = f \tag{1}$$

where m is mass (per unit length), b denotes damping, T denotes tension, EI is the flexural rigidity, and f is the hydrodynamic force (per unit length). The dimensions of Eq. 1 are force per unit length. We expect sinusoidal modes of vibration in time as follows:

$$y(z,t) = Re[Y(z)\ e^{i\omega t}] \tag{2}$$

where $Y(z)$ is the vibration amplitude, and ω is the vibration frequency. For a circular cross section, the strain may be calculated as follows.

$$\frac{\epsilon(z,t)}{R} = \frac{\partial^2}{\partial z^2}[y(z,t)] \tag{3}$$

The hydrodynamic force is modelled as follows:

$$f = Re\left[\left(\frac{1}{4}C_{my}\pi\rho D^2\omega^2 Y + i\frac{1}{2}C_{lv}\rho U^2 D\frac{Y}{|Y|}\right)e^{i\omega t}\right] \tag{4}$$

where ρ is the fluid density, and C_{my} and C_{lv} are the added mass and lift coefficients, respectively. The hydrodynamic coefficients are introduced to the model in the hydrodynamic force and serve as the link between the semiempirical physics-based model and reality.

Introducing Eqs. 2 and 4 into Eq. 1 leads to the following eigenvalue problem, which may be solved to obtain both the vibration frequency and amplitude:

$$\frac{d^2}{dz^2}\left(EI\frac{d^2Y}{dz^2}\right) - \frac{d}{dz}\left(T\frac{dY}{dz}\right) + [-(m+\alpha C_{my})\omega^2 + ib\omega]Y = iC_{lv}qD\frac{Y}{|Y|} \tag{5}$$

where $\alpha = \frac{1}{4}\rho\pi D^2$, and $q = \frac{1}{2}\rho U^2$. Equation 5 is a well-defined nonlinear eigenvalue problem (EVP) with the nonlinearity originating from the dependence of the hydrodynamic coefficients to the frequency ω and the amplitude Y. The EVP may be solved using an iterative nonlinear solver. In this work, the solver VIVA (Triantafyllou et al., 1999) is used. We note that solutions to Eq. 5 need not be mutually orthogonal.

Assuming strip theory (Triantafyllou et al., 1999; Fan, 2019) holds, for an arbitrarily small section of the flexible cylinder's body in VIV, the hydrodynamic coefficients are the same as those of a rigid cylinder undergoing VIV as long as there exists nondimensional similitude. The Buckingham Π theorem dictates that the following nondimensional quantities are relevant:

$$f_r = \frac{\omega D}{2\pi U} \qquad A^* = \frac{A}{D} \qquad Re_D = \frac{UD}{\nu} \tag{6}$$

where f_r is the true reduced frequency; A^* is the nondimensional amplitude; Re_D is the Reynolds number based on diameter; and D, A, and ν stand for the diameter, vibration amplitude, and fluid kinematic viscosity, respectively. The dependence of the hydrodynamic coefficients to the Reynolds number is rather weak and may be neglected (Triantafyllou et al., 1999; Fan, 2019). A hydrodynamic coefficient database is then defined as a map between the following.

$$C_{my} = f(f_r) \qquad C_{lv} = f(f_r, A^*) \tag{7}$$

Assuming strip theory, the hydrodynamic database may be estimated by conducting rigid cylinder-forced vibration experiments and then used to solve the EVP for the flexible body. However, obtaining the hydrodynamic database using systematic experiments is very expensive and time consuming, even for a particular riser configuration; exploring the full space of possible nondimensional amplitudes and true reduced frequencies, accounting for various flow conditions and body geometries, is an impossible task. In this work, we estimate the database by machine learning the hydrodynamic coefficients from experimental data: obtaining the optimal parametric hydrodynamic coefficient database by comparing semiempirical code predictions and observations from experimental data.

Extracting the Hydrodynamic Features (Parametrizing the Hydrodynamic Coefficient Database)

Prior information on the geometry of the hydrodynamic coefficient database, available in literature from experimental studies, was used to extract a set of hydrodynamic features. Specifically, the database obtained by Gopalkrishnan (1993) was used as a starting reference point.

Modelling the added mass coefficient $C_{my} = f(f_r)$ is straightforward, as it can be approximated as a function of a single vari-

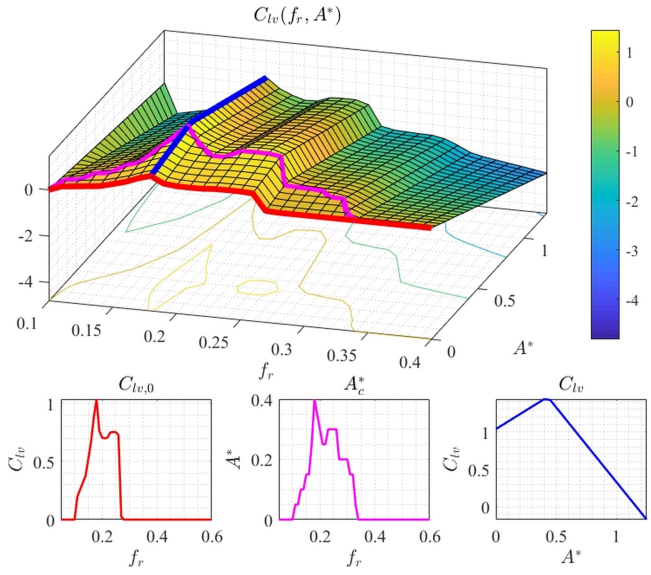

Fig. 1 The Gopalkrishnan (1993) lift coefficient (top) with three highlighted curves used for the database parametrization. The highlighted curves are plotted individually (bottom), where the red line corresponds to the quantity $C_{lv,0} = f(f_r)$ and is the value of the lift coefficient when $A^* = 0$, the purple line corresponds to the quantity $A_c^* = f(f_r)$ and is the critical amplitude where cross sections of the surface parallel to the A^* axis change slope from increasing to decreasing, and the blue line is used to calculate $C_{lv} = f(C_{lv,0}, A_c^*, A^*)$.

able and may be modeled through piecewise linear sections. However, modelling the lift coefficient is more challenging because it is a function of two variables. Figure 1 illustrates the lift coefficient obtained by Gopalkrishnan (1993), which was used as the basis for the parametrization. One may observe that cross sections of the surface parallel to the A^* axis may be represented as piecewise linear curves, which first slope upwards and then downwards. Thus, the cross sections may be modelled leveraging the following: (i) one point $C_{lv,0} = C_{lv}(f_r, 0)$, (ii) the critical amplitude $A_c^* = f(f_r)$ where the cross section changes slope, and (iii) two slopes, one for each piecewise linear section.

Nineteen parameters $\boldsymbol{p} = \{p_i\colon\ i \in [1, 19]\}$ were selected to describe the database as defined by Eq. 7. As indicated, four curves were formulated in particular: C_{my} versus f_r, $C_{lv,0}$ versus f_r, A_c^* versus f_r, and C_{lv} versus A^*, which parametrize the hydrodynamic coefficient database in a reduced order model fashion. The curves may be used to approximate the C_{lv} and C_m, thus allowing one to solve the EVP posed by Eq. 5.

The equations of the mathematical formulation of the parametrization are shown in Appendix A.

Machine-learning Hydrodynamic Coefficient Databases

The end goal of the process is to infer hydrodynamic coefficient databases from the experimental observations. The task may be viewed as a constrained optimization in which the optimal set of parameters $\boldsymbol{p}$ (each constrained in a specific range) that minimize the discrepancy between forward model prediction and observation is searched. The objective function may be formulated as follows:

$$J(\boldsymbol{p}) = \sum_{i=1}^{N_{V_r}} \left[\frac{1}{L} \int_0^L |A_i - \hat{A}_i(\boldsymbol{p})|\, dx + \lambda\, |f_i - \hat{f}_i(\boldsymbol{p})| \right] + R(\boldsymbol{p}) \tag{8}$$

where L is the body's length, N_{V_r} is the number of velocities tested, A denotes amplitude, f denotes frequency, and R denotes a regularization term. The "hat" notation indicates predicted rather than measured quantity. The integral expression ensures that the amplitude discrepancy is minimized across the whole body. The factor λ is chosen arbitrarily.

Given discrete amplitude or strain measurements across the span, the objective function may be formulated as the weighted sum of the root mean square (RMS) error differences between (i) the predicted and observed riser amplitude or strain and (ii) the predicted and observed riser frequency, plus some penalty (regularization) terms.

$$J(\boldsymbol{p}) = \sum_{i=1}^{N_{V_r}} \left[\lambda \sqrt{\frac{1}{N} \sum_{n=1}^{N} [A_{i,n}^* - \hat{A}_{i,n}^*(\boldsymbol{p})]^2} + \sqrt{[f_i - \hat{f}_i(\boldsymbol{p})]^2} \right] + \beta \left[\frac{p_5 - p_1}{0.1} \right]^2 + \gamma |p_{19}| \tag{9}$$

where N is the number of data points along the riser's span, A^* denotes the nondimensional amplitude, and f denotes frequency. The constants λ, β, and γ are chosen arbitrarily, through a trial-and-error approach. The two regularization terms are added to penalize the distance between p_1 and p_5 and the magnitude of the scaling factor of the softplus function.

Obtaining displacement data is usually an expensive process that requires postprocessing of raw measured quantities (usually strain and acceleration), and thus using only sparse raw strain measurements can be advantageous in the sense of eliminating the computational complexity of reconstructing the flexible body's displacement. The objective may then be formulated to accommodate the sparse strain sensing as follows:

$$J(\boldsymbol{p}) = \sum_{i=1}^{N_{V_r}} \left[\lambda \sqrt{\frac{1}{N} \sum_{n=1}^{N} [\boldsymbol{\epsilon}_{i,n} - \hat{\boldsymbol{\epsilon}}_{i,n}(\boldsymbol{p})]^2} + \sqrt{[f_i - \hat{f}_i(\boldsymbol{p})]^2} \right] + \beta \left[\frac{p_5 - p_1}{0.1} \right]^2 + \gamma |p_{19}| \tag{10}$$

where the strain $\boldsymbol{\epsilon}$ is used instead of the amplitude.

The objective function is nonconvex, is nonsmooth, and spans a high-dimensional space. A stochastic coordinate descent algorithm was employed to search the space and return the set of parameters $\boldsymbol{p}$. Specifically, let

$$\boldsymbol{p} = (p_1, p_2, ..., p_{18}, p_{19}) \tag{11}$$

be the vector representation of the parametric space. For n iterations, the parameters were updated according to the following rule:

$$\boldsymbol{p}_{n+1} = \boldsymbol{p}_n + \delta_i \boldsymbol{v}_i \tag{12}$$

where the step size δ_i was selected as the following.

$$\begin{aligned} &\delta_i = \underset{\delta\ \in\ \Delta}{\arg\min}\ J(\boldsymbol{p} + \delta \boldsymbol{v}_i) \\ &\Delta = \{0, s_1, s_2, .., s_n \mid s_i \sim \mathrm{N}(0, \sigma)\}, \\ &\sigma \propto \exp(-i) \end{aligned} \tag{13}$$

The descent direction $\boldsymbol{v}_i$ was selected as either a random binary vector (similar approach to a coordinate descent) with some prob-

ability or as a random unit vector the rest of the times. Specifically, we have the following.

$$\begin{aligned} &\boldsymbol{v}_i = (v_1, v_2, ..., v_{18}, v_{19}) \mid v_i \sim \mathrm{U}(\{0,1\}) \ \vee \\ &\boldsymbol{v}_i = (v_1, v_2, ..., v_{18}, v_{19}) \mid |\boldsymbol{v}_i| = 1 \ \wedge \ v_i \in \mathbb{R} \end{aligned} \tag{14}$$

The algorithm was performed on the transformed set of variables $\boldsymbol{q}$ defined as follows:

$$q_i = \sigma^{-1}\left(\frac{p_i - p_{i,\min}}{p_{i,\max} - p_{i,\min}}\right) \tag{15}$$

where σ is the sigmoid function. The capabilities of the algorithm are demonstrated in the following section, although there exists no theoretical foundation guaranteeing global optimality of the returned parameters.

RESULTS AND DISCUSSION

The framework was used in conjunction with the semiempirical prediction program VIVA (Triantafyllou et al., 1999; Zheng et al., 2011) to extract the optimal hydrodynamic databases (i.e., train database models) according to Eqs. 9 and 10 from various observed VIV response data sets.

Initial Condition

Defining a suitable initial condition for the optimization was deemed appropriate because initializing at random would, in the least, slow down the convergence of the optimization algorithm. The physics-informed database obtained by Gopalkrishnan (1993) via rigid cylinder-forced vibration experiments was selected as the appropriate initial condition.

To determine the set of initial parameters $\boldsymbol{p}_0$ that optimally parametrize the Gopalkrishnan (1993) database, an optimization problem was formulated to minimize the discrepancy between the $C_{lv} = f(f_r, A^*)$ of the Gopalkrishnan database and the initial parametric database defined by $\hat{C}_{lv} = f(f_r, A^*, \boldsymbol{p}_0), \hat{C}_m = f(f_r, \boldsymbol{p}_0)$. The objective function to be minimized in this context may be formulated as follows.

$$\begin{aligned} &J(\boldsymbol{p}) \\ &= \int_{A^*_{\min}}^{A^*_{\max}} \int_{f_{r_{\min}}}^{f_{r_{\max}}} |C_{lv}(f_r, A^*) - \hat{C}_{lv}(f_r, A^*, \boldsymbol{p})| df_r dA^* + R(\boldsymbol{p}) \end{aligned} \tag{16}$$

In a discrete fashion, the objective may be rewritten as in the following, adding a regularization term penalizing the magnitude of the softplus function.

$$J(\boldsymbol{p}) = \sum_{i=1}^{N_{A^*}} \sum_{j=1}^{N_{f_r}} \frac{\sqrt{[C_{lv}(f_{r_j}, A^*_i) - \hat{C}_{lv}(f_{r_j}, A^*_i, \boldsymbol{p})]^2}}{N_{f_{r_j}} \cdot N_{A^*_i}} + \beta |p_{19}| \tag{17}$$

where N_{A^*} and N_{f_r} are number of nondimensional amplitudes and the number of reduced frequencies used, respectively. The value of the parameter β was chosen arbitrarily. The resulting C_{lv} contour as well as the training contour is shown in Fig. 2.

The resulting initial condition qualitatively agrees with the training database in terms of both magnitude and contour shape (especially in the $f_r \in [0.15, 0.30]$ range) where most observed VIV responses occur.

The selected database parametrization offers flexibility in terms of capturing the two "peak" contours of the training database, parametrizing those as piecewise linear curves. It should be noted that the initial condition only serves as the starting point for the database learning problem, and further refinement follows during the training stage of the process.

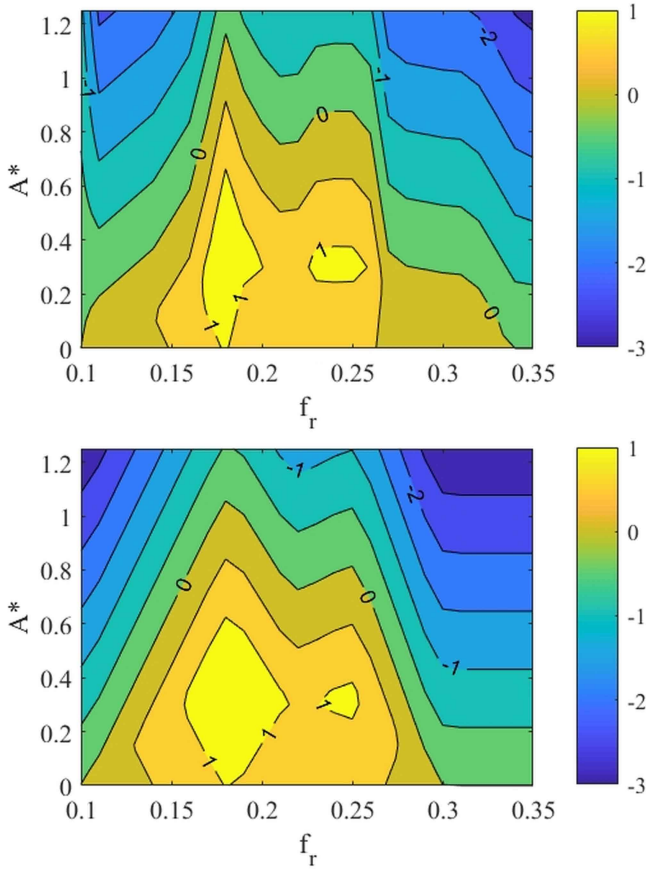

Fig. 2 Initial condition for the parametric database; the Gopalkrishnan (1993) database lift coefficient was used as the reference starting point. Top: lift coefficient contour of the Gopalkrishnan database; bottom: lift coefficient contour of the parametric database obtained as the initial condition. An optimization problem was formulated to find the parameters that optimally approximate the Gopalkrishnan database lift coefficient. The parametric framework allows for a (smoothed) piecewise linear approximation of the Gopalkrishnan database.

Vertical Riser in Uniform Flow Using Sparse Strain Sensing

The first application of the framework was extracting the database from experimental data obtained as part of the Norwegian Deepwater Programme (NDP) (Braaten and Lie, 2004). A flexible cylinder with length-over-diameter ratio $L/D \approx 1{,}400$ was towed at Reynolds numbers $Re_D \approx 7.1 \cdot 10^3$ to $5.7 \cdot 10^4$. Tested velocities were in the range of 0.3 to 2.4 m/s.

Although training was done using sparse strain data, the accuracy of the database and forward model was validated against experimental displacement and frequency data (rather than strain data), which were of interest. To avoid any confusion, in this context, the terms "riser," "flexible riser," and "flexible cylinder" refer to the riser model used in the NDP experiments and are not to be confused with the industry standard *flexible riser* meaning composite pipe. The amplitude response results are shown in Fig. 3, and the frequency response results are shown in Fig. 4.

After training, there is agreement between experimental observation and forward model prediction both in terms of amplitude

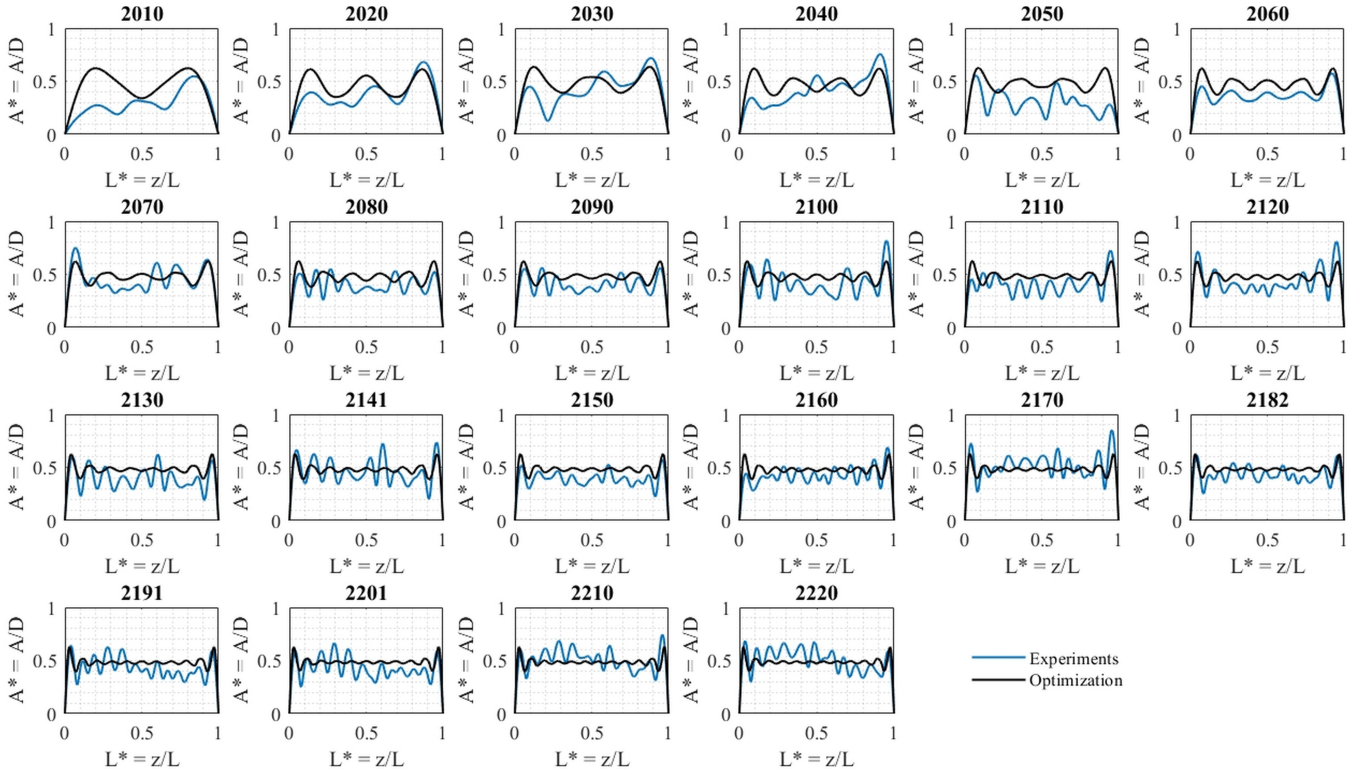

Fig. 3 Vertical riser in uniform flow amplitude response: Temporal RMS nondimensional amplitude (y axis) as a function of span (x axis) is shown for various flow velocities (range: 0.3–2.4 m/s). Each subplot (titled with an associated number from the NDP experiments) corresponds to a different incoming flow velocity; a higher experiment number corresponds to a higher flow velocity. Experimentally observed (reconstructed) amplitude is shown as a solid blue line, and predictions using the data-informed forward model are shown as a solid black line. Training was done using sparse strain measurements along the body. Reasonably accurate predictions are made especially as the flow velocity increases and experimental imperfections (manifesting as response asymmetries) become negligible.

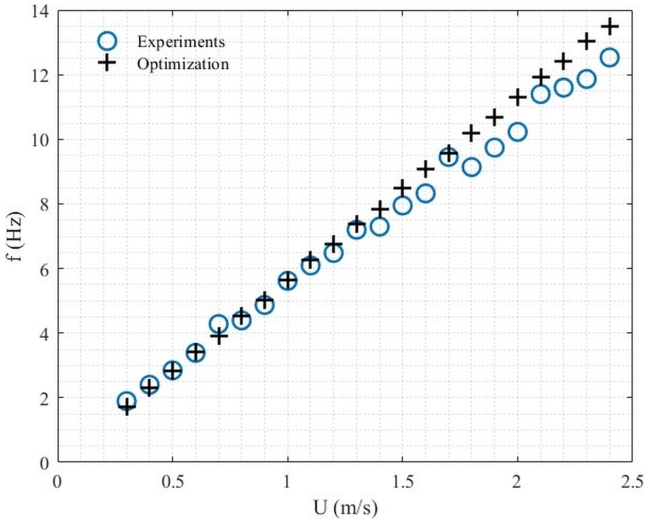

Fig. 4 Vertical riser in uniform flow frequency response: Vibration frequency (y axis) is plotted against flow velocity (x axis).

as a function of span and in terms of frequency as a function of incoming flow velocity. This result demonstrates how databases need not be inferred from displacement data, which are rather expensive to obtain, but may be determined directly from sparse strain measurements along the structure, which are in practice easier to obtain, especially in uncontrolled environments and in the field.

Figure 3 illustrates the amplitude response prediction results. The amplitude is approximated to reasonable accuracy, especially for high flow velocities where the observed responses are rather symmetrical, as expected in theory.

Cases 2010 to 2040 in the amplitude response (Fig. 3) demonstrate how the experimental results behave unexpectedly at low flow velocities, because a nonsymmetric response is observed in a symmetric problem: a vertical uniform riser within a uniform flow. Although a symmetric response might be expected, because the governing equation does not accept asymmetric solutions for symmetric loading, the symmetry is broken by the generation of standing and traveling waves along the riser; small perturbations in the oncoming current determine the direction of the traveling waves that break the symmetry. Hence, the direction of travel is "random" and can be reversed when repeating experiments.

As is illustrated in Fig. 4, the predicted frequency as a function of incoming flow velocity is reasonably accurate across the full range of flow velocities, with a deviation of at most 15% observed at high flow speeds.

Vertical Riser in Stepped Current

In this case, a vertical uniform tensioned flexible riser was placed in a stepped incoming flow stream. Accordingly, only half of the riser's span was exposed to the flow stream (the exposed half saw a uniform flow), whereas the rest of the body was immersed in still water.

The data were collected by Chaplin, Bearman, Huera Huarte, et al. (2005) and were also later used for blind predictions in Chaplin, Bearman, Cheng, et al. (2005). The riser's length was

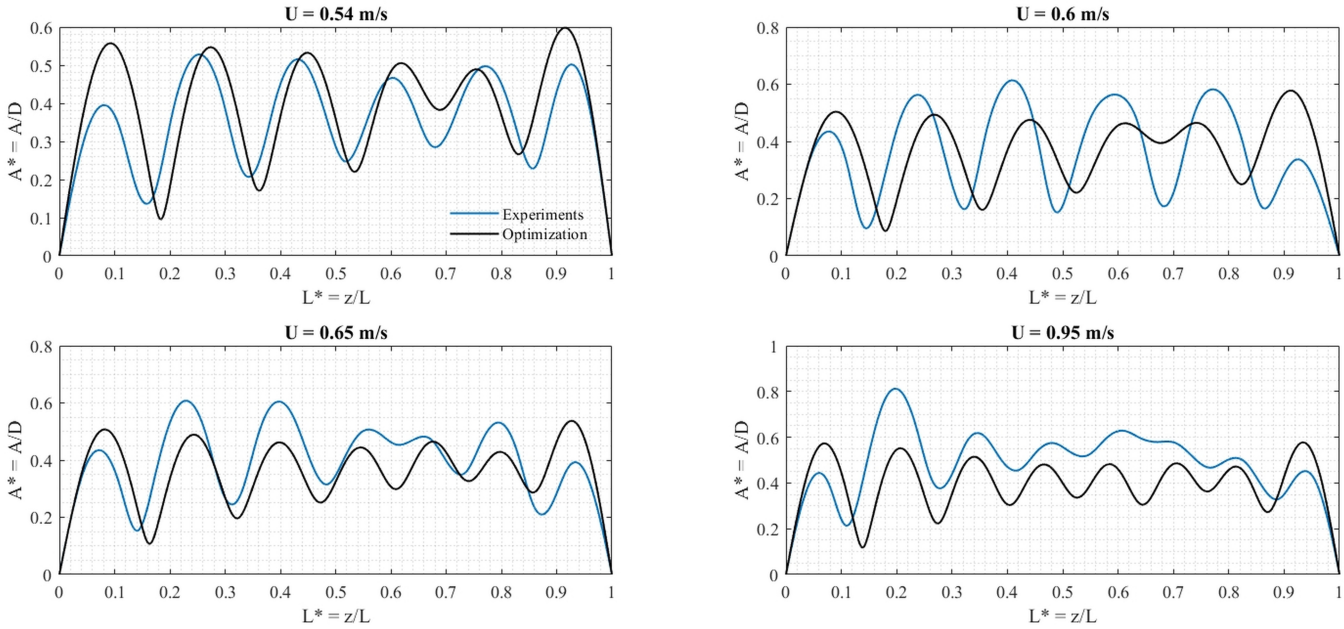

Fig. 5 Vertical riser in stepped current amplitude response: Temporal RMS nondimensional amplitude (y axis) as a function of span (x axis) is shown for four tested velocities, where the experimentally observed (reconstructed) amplitude is shown as a solid blue line, and the prediction using the trained forward model is shown as a solid black line.

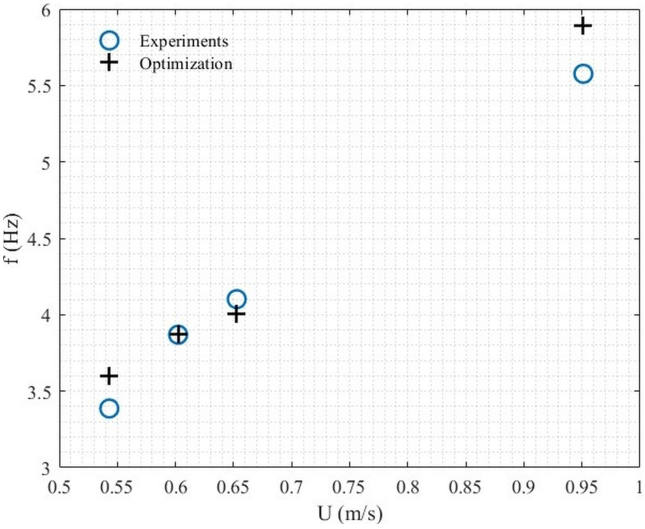

Fig. 6 Vertical riser in stepped current frequency response: Vibration frequency (y axis) is plotted against flow velocity (x axis), where blue circles are the experimentally observed frequencies, and black crosses are the predicted frequencies.

$L = 13.12$ m, with a length-over-diameter ratio of $L/D \approx 450$. The velocities tested were $U = 0.54$ m/s, $U = 0.60$ m/s, $U = 0.65$ m/s, and $U = 0.95$ m/s. The corresponding Reynolds numbers were in the range of $Re_D \approx 13 \cdot 10^3$ to $23 \cdot 10^3$.

Given the lower length-over-diameter ratio of this set of experiments compared with the NDP experiments ($L/D \approx 1{,}500$), a lower mode number was expected (and observed) experimentally; the maximum mode number was 8. Training on this data set was done using reconstructed displacement data and according to Eq. 9.

The amplitude responses after training on the four tested velocities are shown in Fig. 5. As the figure illustrates, the forward model using the extracted hydrodynamic coefficient database makes reasonably accurate predictions of the amplitude response, with both the magnitude and mode shapes reasonably accurately estimated. Additionally, the prediction of the mode number (i.e., 6, 6, 7, and 8) was correct in all cases, with the locations of the peaks predicted to within 15% of their true locations.

Figure 6 shows the frequency predictions. As is evident in the figure, the data-informed forward model can make frequency predictions with relative errors not exceeding 10%.

Catenary Riser in Uniform Flow

Catenary type risers and pipes are the most commonly used in offshore applications. In addition, flexible offshore equipment such as mooring lines assume catenary shapes when operating while also affected by VIV. Predicting the response of a catenary riser poses significant challenges as the flow velocity normal to the flexible body varies as a function of span (geometric curvature needs to be considered) and the tension varies significantly along the body. In the case where there is an oblique angle between the incoming flow stream and the catenary plane three dimensional effects also become significant.

For this analysis, experimental data of catenary riser VIV responses from experiments conducted as part of the NDP (Lie, 2001) were used. Specifically, a model catenary riser spanning a length $L = 12.5$ m, with a length-over-diameter ratio $L/D \approx 900$ was towed at speeds ranging from 0.12 m/s to 0.36 m/s. The incidence angle between the catenary plane and the incoming flow was either 0 degrees (i.e., the catenary plane was aligned with the flow) or 30 degrees (the catenary plane was oriented at an oblique angle with respect to the incoming flow). The Reynolds numbers were in the range $Re_D \approx 1.5 \cdot 10^3$ to $4.2 \cdot 10^3$.

In this and the following sections, the terms “catenary riser" and “SCR riser" (the usual industry abbreviation for a steel catenary riser) will be used interchangeably and refer to the catenary riser model used in the NDP experiments.

Incidence Angle: 0 Degrees. In this case, the incidence angle between the catenary plane and the incoming flow stream was

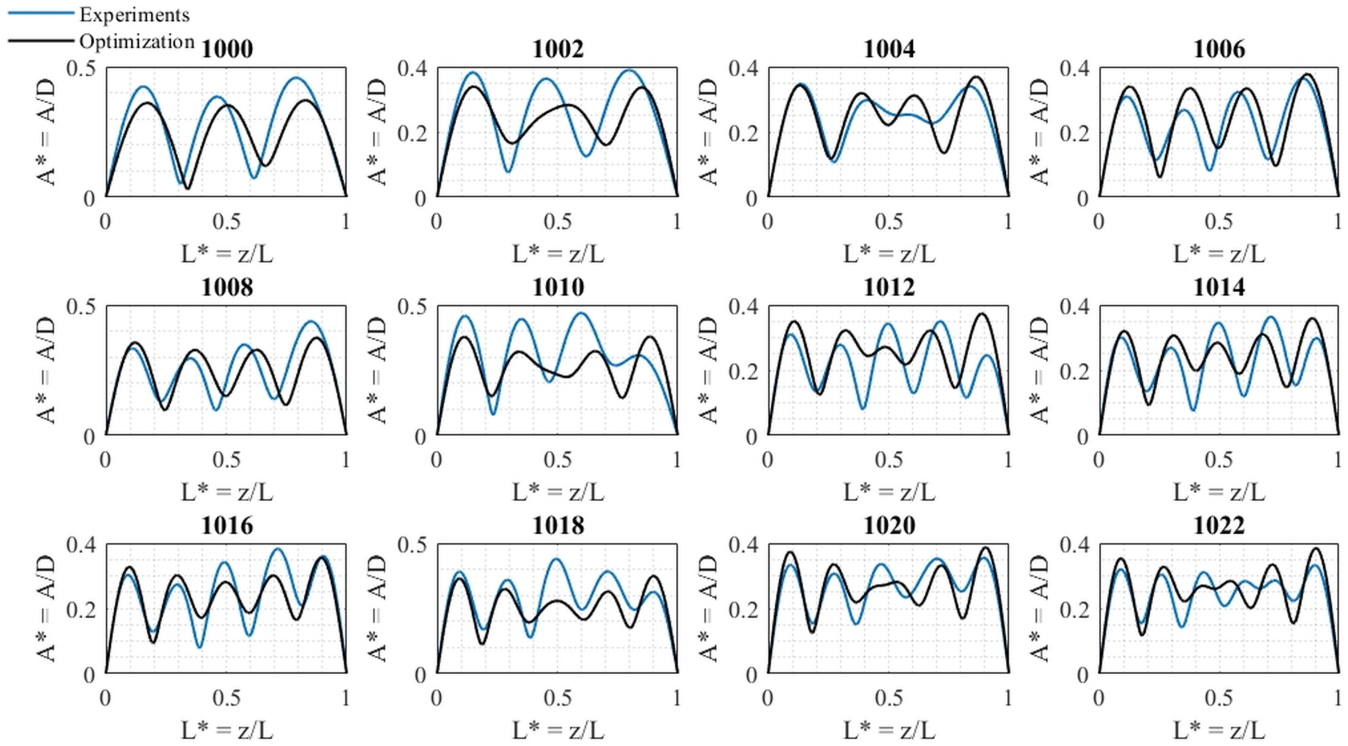

Fig. 7 Catenary riser (curved geometry) in uniform flow (catenary plane parallel to the incoming flow) amplitude response. Temporal RMS nondimensional amplitude (y axis) as a function of span (x axis) shown for various flow velocities (range: 0.12–0.36 m/s). Each subplot (titled with an associated number from the NDP experiments) corresponds to a different incoming flow velocity; a higher experiment number corresponds to a higher flow velocity. Experimentally observed (reconstructed) amplitudes are shown as a solid blue line, and predictions are shown as a solid black line.

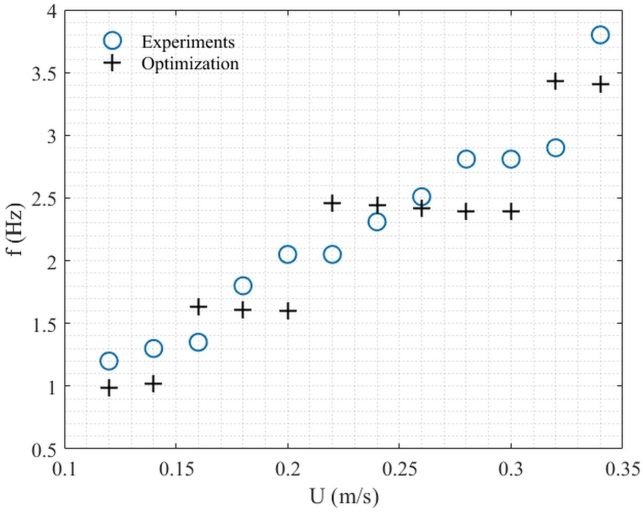

Fig. 8 Catenary riser (curved geometry) in uniform flow (incidence angle: 0 degree) frequency response. Vibration frequency (y axis) is plotted against flow velocity (x axis), where blue circles are the experimentally observed frequencies, and black crosses are the predicted frequencies.

0 degrees; that is, the catenary plane was aligned with the flow. Although the geometric curvature was signficant, three-dimensional (3D) effects were negligible.

The results for the amplitude prediction are shown in Fig. 7. As is evident in the figure, the learned optimal parametric hydrodynamic coefficient database can reasonably accurately predict the amplitude response of the SCR riser. Moreover, not only is the amplitude magnitude accurately predicted across the whole body's span but also the mode number and mode shape are also accurately predicted.

The frequency response is shown in Fig. 8. As Fig. 8 illustrates, the frequency response prediction is not as compelling as the amplitude prediction, albeit reasonable, although in terms of absolute magnitude, the predicted frequencies are fewer than a single unit off compared with predictions. It appears as if the trend of the observed data is not very well captured by the prediction. The predicted frequency "jumps" correspond to an increase in the mode number of the amplitude response and are expected in theory. For example, from steam velocities $U = 0.14$ m/s (experiment no. 1002) to $U = 0.16$ m/s (experiment no. 1004), the mode number changes from 3 to 4, and a frequency "jump" is expected. The observed results, however, show a more gradual (almost linear) increasing trend in the frequency.

Incidence Angle: 30 Degrees. In this case, the incidence angle between the catenary plane and the incoming flow stream was 30 degrees. Three-dimensional effects as well as curvature effects were superimposed. Note that the cross-flow direction remains unchanged and is defined as the direction perpendicular to the flow, rather than the direction perpendicular to the catenary plane.

The amplitude response of the SCR riser at a 30-degree incidence angle between the catenary plane and the flow is shown in Fig. 9. As is evident in the figure, the hydrodynamic coefficient database extracted from the 30-degree incidence angle data set is competent in predicting the amplitude response of the SCR riser both in terms of amplitude and in terms of mode number. The

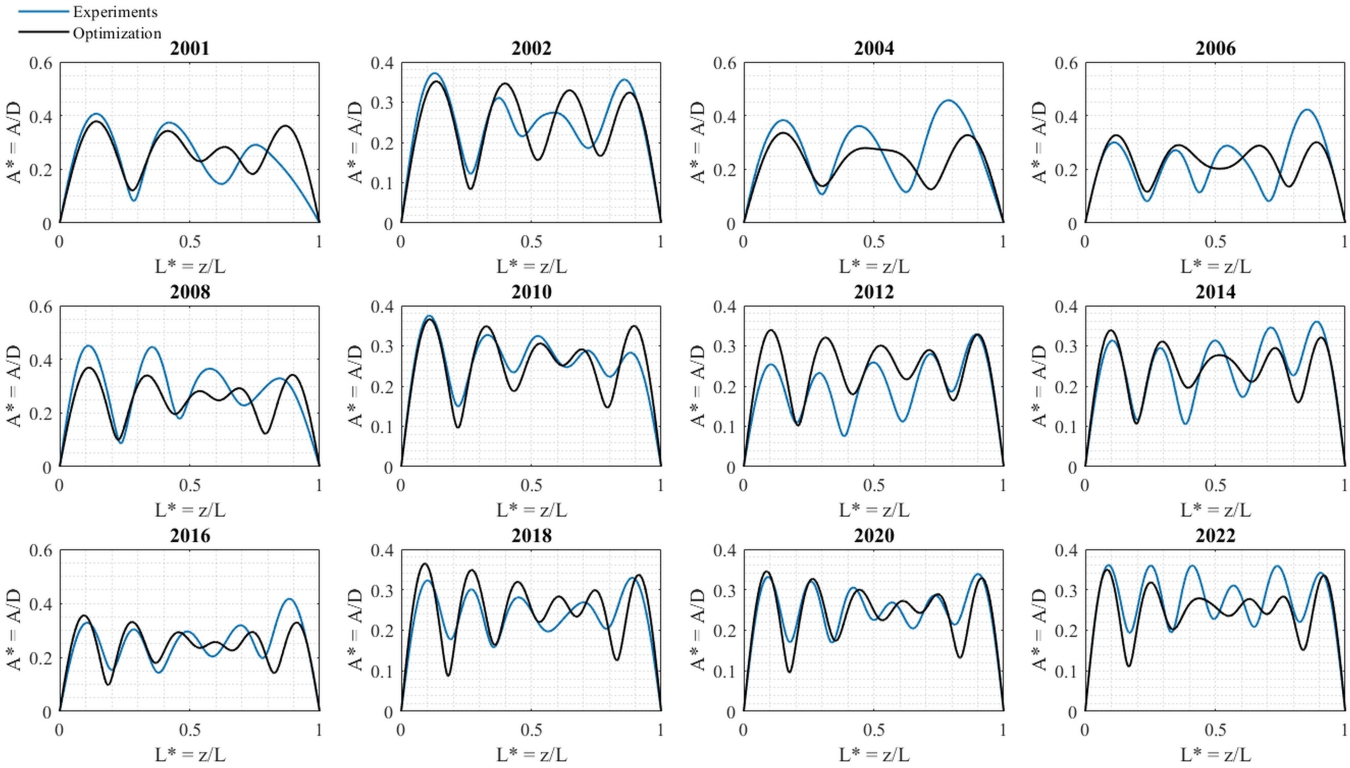

Fig. 9 Catenary riser (curved geometry) in uniform flow: The catenary plane was oriented at a 30-degree incidence angle with respect to the incoming flow, and thus both curvature and 3D effects were significant. Temporal RMS nondimensional amplitude (y axis) as a function of span (x axis) is shown for various flow velocities. Each subplot (titled with an associated number from NDP experiments) corresponds to a different incoming flow velocity; a higher experiment number corresponds to a higher flow velocity. Experimentally observed (reconstructed) amplitude is shown as a solid blue line, and predictions are shown as a solid black line.

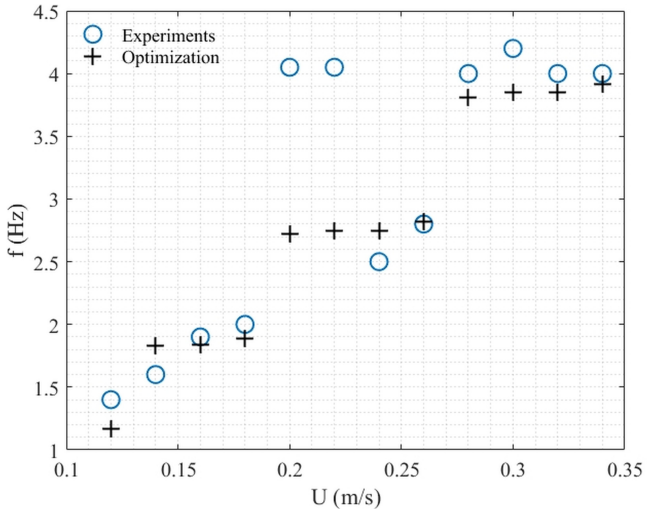

Fig. 10 Catenary riser (curved geometry) in uniform flow: The catenary plane was oriented at a 30-degree incidence angle with respect to the incoming flow, and thus both curvature and 3D effects were significant. Vibration frequency (y axis) is plotted against flow velocity (x axis). Blue circles are the experimentally observed frequencies, and black crosses are the predicted frequencies. Two outlier points from experiments are evident but were not excluded from training or prediction.

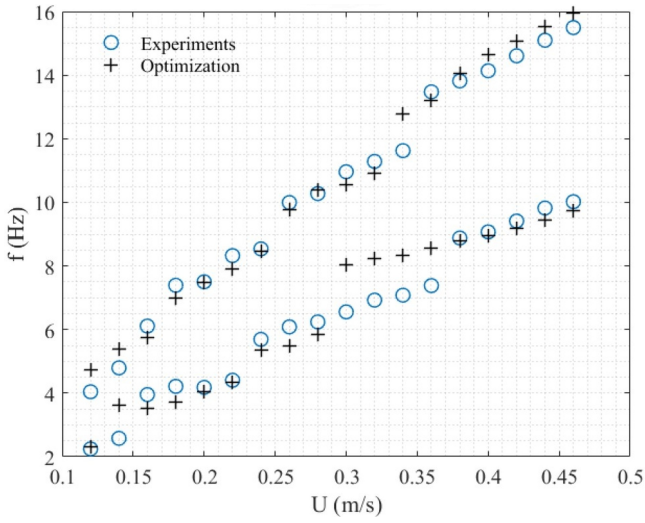

Fig. 11 Stepped (two-diameter) riser in uniform flow: The cylinder is undergoing dual-frequency vibrations (i.e., two distinct vibrations coexist on the structure at the same time). Vibration frequencies (y axis) measured are plotted against flow velocity (x axis), where blue circles are the experimentally observed frequencies, and black crosses are the predicted frequencies. The predictions are made using two databases, one for each distinct diameter region.

mode shape is also reasonably accurately predicted. Specifically, the mode number is correctly predicted to within 1 in all cases, and the asymmetry of the response, which was expected in the experiments because the flow velocity as seen by the riser changes as a function of its span, is well captured, with peak locations predicted reasonably accurately.

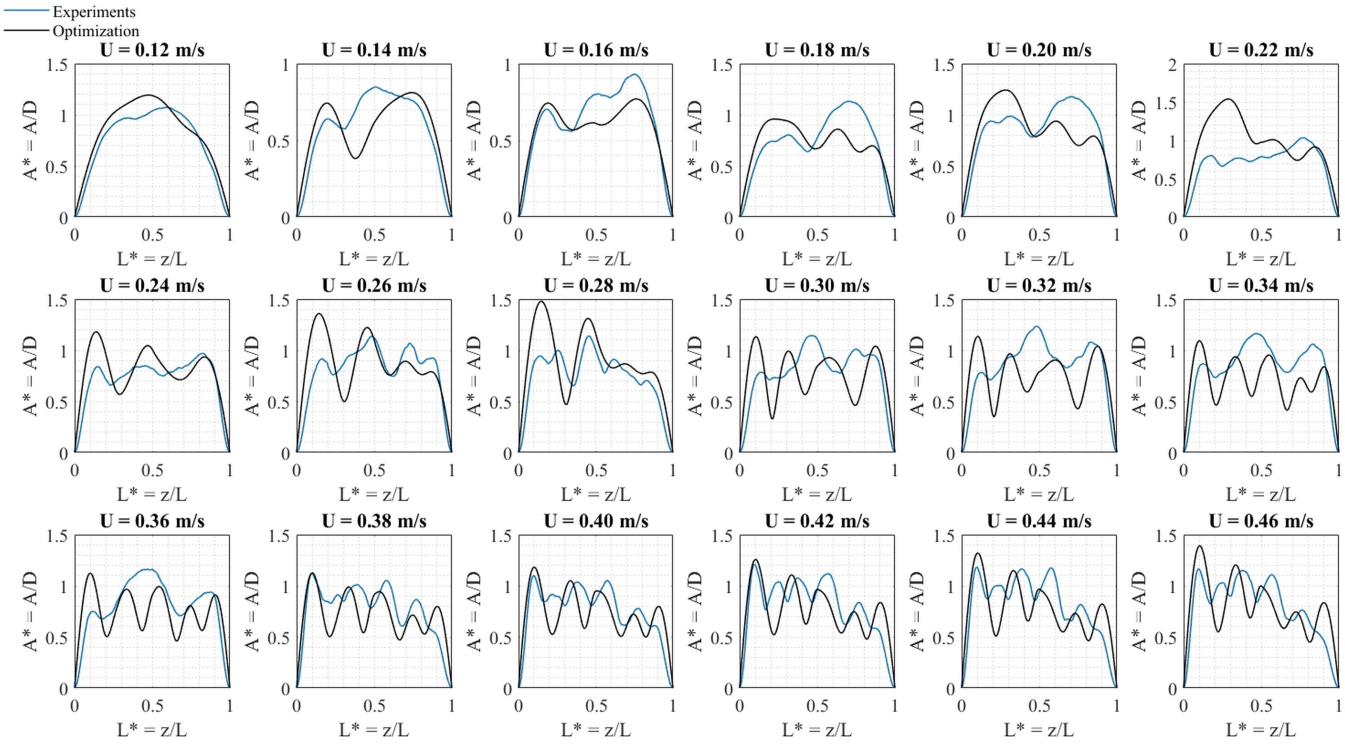

Fig. 12 Stepped (two-diameter) riser in uniform flow: The cylinder is undergoing dual-frequency vibrations (i.e., two distinct vibrations coexist on the structure at the same time). Temporal RMS nondimensional amplitude (y axis) as a function of span (x axis) is shown for various flow velocities. Experimentally measured amplitude is shown as a solid blue line, and prediction is shown as a solid black line. The predictions are made using two databases, one for each distinct diameter region.

The frequency response results are shown in Fig. 10. As Fig. 10 illustrates, the frequency prediction approximated the experimental observations to reasonable accuracy. The two discrepancies for flow velocities $U = 0.20$ m/s and $U = 0.22$ m/s are outlier points and are probably caused by a fault in measurement. However, it was decided to not exclude them from the predictions or the training process to see how outlier points affect the training, which was also done a second time, excluding the outliers. The predictions with or without the outliers were almost the same.

Stepped Riser in Uniform Flow

Relatively few things are known about VIV of risers with distinct diameters across the span. For the purpose of this work, experimental data obtained by Fan (2019) were used. A flexible cylinder with two distinct diameters measuring $d = d_1 = 5$ mm and $d_2 = 8$ mm, each spanning half the cylinder's total length of $L = 1.22$ m, was used. The length-over-diameter ratio for the riser was $L/D \approx 250$. Tested velocities were in the range $U = 0.12$ ms to 0.46 m/s. Reynolds numbers were in the range $Re_D \approx 500$ to 2,000.

The structural response reported by Fan (2019) and confirmed by A Li et al. (2022) is complex in the sense that two distinct frequency vibrations coexist on the structure at the same time. The dual-frequency vibration, identified via wavelet synchrosqueezed transform, manifests as two distinct travelling wave responses induced on the cylinder (initiated at the two distinct diameter regions) which propagate along the structure.

To account for the dual-frequency vibrations, two parametric hydrodynamic coefficient databases were used for the learning problem. Although the two databases were of the same parametric form (as described earlier), each database was used to predict the response of a separate half of the riser (corresponding to a separate diameter). Training of the two databases was done according to Eq. 9 in a sequential fashion, optimizing each database given the other constant and alternating between the two. Therefore, to solve the EVP and obtain the amplitude and frequency response, a distinct parametric hydrodynamic coefficient database was used for each half of the riser, making the problem highly nonlinear. The identified dominant and subdominant frequencies of the EVP were then used to predict the two distinct observed frequencies.

Figure 11 shows the two distinct frequency predictions as well as the experimentally observed frequencies. As is evident in the figure, the data-informed model can reasonably accurately predict both frequencies while overestimating the low frequencies at the mode transition window where $U \approx 0.30$ to 0.35 m/s.

Figure 12 illustrates the predicted amplitude responses along with the observed responses. It is worth noting that those are highly asymmetric and more complex than those observed for vertical or catenary risers. Nonetheless, with the exception of the mode transition region at flow velocities $U \approx 0.30$ to 0.35 m/s, the overall mode shape and trend of the response is reasonably accurately captured, and the magnitude is adequately predicted.

CONCLUSIONS

A framework following the paradigm of Rudy et al. (2022) has been used that, in conjunction with a forward VIV predictive model such as VIVA (Triantafyllou et al., 1999), may be able to extract hydrodynamic coefficient databases from VIV response data—a task that used to be intractable given the number of experiments required via rigid cylinder-forced vibrations.

The capability of the framework to extract databases is being demonstrated for vertical flexible risers in uniform or stepped

flow, catenary risers in uniform flow, and stepped risers in uniform flow. In addition, the framework is extended to using only sparse raw sensor measurements. Last but not least, an appropriate physics-informed initialization for the database optimization problem has also been determined.

The capability of the forward model to make predictions after the hydrodynamic coefficient database extraction suggests that the underlying physics may be encoded in the learned databases, providing ample opportunity for further exploration. An easily identified research direction remains—physically interpreting the acquired hydrodynamic coefficient databases.

A final remark is that extracting a hydrodynamic database requires approximately one day, whereas each individual prediction (of amplitude and frequency response for a single flow velocity) with a trained database requires less than a few seconds. With its reasonably accurate prediction capabilities, this physics-based and data-informed model is able to make predictions comparable with much higher-fidelity models of greater complexity and computational cost.

ACKNOWLEDGEMENTS

The authors acknowledge support from the DigiMaR (Digital Twin for Marine Riser) consortium, MathWorks, and the Onassis Foundation.

REFERENCES

Baek, H, and Karniadakis, GE (2009). "Suppressing Vortex-induced Vibrations via Passive Means," *J Fluids Struct*, 25(5), 848–866. https://doi.org/10.1016/j.jfluidstructs.2009.02.006.

Bearman, PW (2011). "Circular Cylinder Wakes and Vortex-induced Vibrations," *J Fluids Struct*, 27(5–6), 648–658. https://doi.org/10.1016/j.jfluidstructs.2011.03.021.

Bernitsas, MM, Ofuegbe, J, Chen, JU, and Sun, H (2019). "Eigensolution for Flow Induced Oscillations (VIV and Galloping) Revealed at the Fluid-structure Interface," *Proc 2019 38th Int Conf Offshore Mech Arct Eng*, Glasgow, UK, ASME, 2, 352–365. https://doi.org/10.1115/OMAE2019-96823.

Bernitsas, MM, and Raghavan, K (2008). "Reduction/suppression of VIV of Circular Cylinders through Roughness Distribution at $8 \times 10^3 < Re < 1.5 \times 10^5$," *Proc 2008 27th Int Conf Offshore Mech Arct Eng*, Estoril, Portugal, ASME, 5, 1001–1005. https://doi.org/10.1115/OMAE2008-58024.

Braaten, H, and Lie, H (2004). *NDP Riser High Mode VIV Tests Main Report*, Report, MARINTEK, Trondheim, Norway.

Chaplin, JR, Bearman, PW, Cheng, Y, et al. (2005). "Blind Predictions of Laboratory Measurements of Vortex-induced Vibrations of a Tension Riser," *J Fluids Struct*, 21(1), 25–40. https://doi.org/10.1016/j.jfluidstructs.2005.05.016.

Chaplin, JR, Bearman, PW, Huera Huarte, FJ, and Pattenden, RJ (2005). "Laboratory Measurements of Vortex-induced Vibrations of a Vertical Tension Riser in a Stepped Current," *J Fluids Struct*, 21(1), 3–24. https://doi.org/10.1016/j.jfluidstructs.2005.04.010.

Evangelinos, C, Lucor, D, and Karniadakis, GE (2000). "DNS-derived Force Distribution on Flexible Cylinders Subject to Vortex-induced Vibration," *J Fluids Struct*, 14(3), 429–440. https://doi.org/10.1006/jfls.1999.0278.

Fan, D (2019). *Mapping the Hydrodynamic Properties of Flexible and Rigid Bodies Undergoing Vortex-induced Vibrations*, Doctoral thesis, Massachusetts Institute of Technology, Cambridge, MA, USA, 243 pp. https://dspace.mit.edu/handle/1721.1/122133.

Fan, D, Jodin, G, et al. (2019). "A Robotic Intelligent Towing Tank for Learning Complex Fluid-structure Dynamics," *Sci Rob*, 4(36), eaay5063. https://doi.org/10.1126/scirobotics.aay5063.

Fan, D, and Triantafyllou, MS (2017). "Vortex Induced Vibration of Riser with Low Span to Diameter Ratio Buoyancy Modules," *Proc 27th Int Ocean Polar Eng Conf*, San Francisco, CA, USA, ISOPE, 3, 1151–1159.

Fan, D, Wang, Z, Triantafyllou, MS, and Karniadakis, GE (2019). "Mapping the Properties of the Vortex-induced Vibrations of Flexible Cylinders in Uniform Oncoming Flow," *J Fluid Mech*, 881, 815–858. https://doi.org/10.1017/jfm.2019.738.

Fan, D, Wu, B, Bachina, D, and Triantafyllou, MS (2019). "Vortex-induced Vibration of a Piggyback Pipeline Half Buried in the Seabed," *J Sound Vib*, 449, 182–195. https://doi.org/10.1016/j.jsv.2019.02.038.

Gopalkrishnan, R (1993). *Vortex-induced Forces on Oscillating Bluff Cylinders*, Doctoral thesis, Massachusetts Institute of Technology, Cambridge, MA, USA, 247 pp.

Govardhan, R, and Williamson, CHK (2002). "Resonance Forever: Existence of a Critical Mass and an Infinite Regime of Resonance in Vortex-induced Vibration," *J Fluid Mech*, 473, 147–166. https://doi.org/10.1017/S0022112002002318.

Han, Q, Ma, Y, Xu, W, Fan, D, and Wang, E (2018). "Hydrodynamic Characteristics of an Inclined Slender Flexible Cylinder Subjected to Vortex-induced Vibration," *Int J Mech Sci*, 148, 352–365. https://doi.org/10.1016/j.ijmecsci.2018.09.010.

Hover, FS, Tvedt, H, and Triantafyllou, MS (2001). "Vortex-induced Vibrations of a Cylinder with Tripping Wires," *J Fluid Mech*, 448, 175–195. https://doi.org/10.1017/S0022112001005985.

Kharazmi, E, Fan, D, Wang, Z, and Triantafyllou, MS (2021). "Inferring Vortex Induced Vibrations of Flexible Cylinders Using Physics-informed Neural Networks," *J Fluids Struct*, 107, 103367. https://doi.org/10.1016/j.jfluidstructs.2021.103367.

Kharazmi, E, Wang, Z, et al. (2021). "From Data to Assessment Models, Demonstrated through a Digital Twin of Marine Risers," *Proc Offshore Technol Conf*, Houston, TX, USA, Offshore Technology Conference, OTC-30985-MS. https://doi.org/10.4043/30985-MS.

Larsen, CM, Vikestad, K, Yttervik, R, Passano, E, and Baarholm, GS (2001). *VIVANA Theory Manual*, MARINTEK, Trondheim, Norway.

Li, A, Mentzelopoulos, A, Triantafyllou, MS, and Fan, D (2022). "Dual-frequency Vortex-induced Vibrations of Long Flexible Stepped Cylinders," *Phys Fluids*, 34, 075105. https://doi.org/10.1063/5.0098391.

Li, N, Park, H, Sun, H, and Bernitsas, MM (2022). "Hydrokinetic Energy Conversion Using Flow Induced Oscillations of Single-cylinder with Large Passive Turbulence Control," *Appl Energy*, 308, 118380. https://doi.org/10.1016/j.apenergy.2021.118380.

Lie, H (2001). *NDP VIV Model Test of a Catenary Riser - STRIDE Ph.4*, Technical report, MARINTEK, Trondheim, Norway.

Ma, L (2022). "Interpretable Machine Learning for Insight Extraction from Rigid Cylinder Flow-induced Vibration Phenomena," *Appl Ocean Res*, 119, 102975. https://doi.org/10.1016/j.apor.2021.102975.

Ma, L, Lin, K, Fan, D, Wang, J, and Triantafyllou, MS (2022). "Flexible Cylinder Flow-induced Vibration," *Phys Fluids*, 34(1), 011302. https://doi.org/10.1063/5.0078418.

Ma, L, Resvanis, TL, and Vandiver, JK (2022). "Understanding the Higher Harmonics of Vortex-induced Vibration Response Using a Trend-constrained, Machine Learning Approach," *Mar Struct*, 83, 103195. https://doi.org/10.1016/j.marstruc.2022.103195.

Meng, X, Wang, Z, Fan, D, Triantafyllou, MS, and Karniadakis, GE (2021). "A Fast Multi-fidelity Method with Uncertainty Quantification for Complex Data Correlations: Application to Vortex-induced Vibrations of Marine Risers," *Comput Methods Appl Mech Eng*, 386, 114212. https://doi.org/10.1016/j.cma.2021.114212.

Mentzelopoulos, A, et al. (2022). "Inferring Optimal Hydrodynamic Databases for Vortex Induced Cross Flow Vibration Prediction of Marine Risers Using Limited Sensor Measurements," *Proc 32nd Int Ocean Polar Eng Conf*, Shanghai, China, ISOPE, 3, 2037–2043.

Park, H, Kumar, RA, and Bernitsas, MM (2016). "Suppression of Vortex-induced Vibrations of Rigid Circular Cylinder on Springs by Localized Surface Roughness at $3 \times 10^4 \leq Re \leq 1.2 \times 10^5$," *Ocean Eng*, 111, 218–233. https://doi.org/10.1016/j.oceaneng.2015.10.044.

Passano, E, Larsen, CM, Lie, H, and Wu, J (2016). *VIVANA—Theory Manual Version 4.8*, Norwegian University of Science and Technology, Trondheim, Norway.

Raghavan, K, and Bernitsas, MM (2011). "Experimental Investigation of Reynolds Number Effect on Vortex Induced Vibration of Rigid Circular Cylinder on Elastic Supports," *Ocean Eng*, 38(5–6), 719–731. https://doi.org/10.1016/j.oceaneng.2010.09.003.

Resvanis, TL, and Vandiver, JK (2017). "Response Variability in Flexible Cylinder VIV Model Test Data," *Proc 2017 36th Int Conf Ocean Offshore Arct Eng*, Trondheim, Norway, ASME, 2, V002T08A035. https://doi.org/10.1115/OMAE2017-61516.

Resvanis, TL, and Vandiver, JK (2022). "Efficient Measurement of Hydrodynamic Coefficients for Vibrating Cylinders at Supercritical Reynolds Numbers," *J Fluids Struct*, 108, 103427. https://doi.org/10.1016/j.jfluidstructs.2021.103427.

Resvanis, TL, Vandiver, JK, and Fu, S (2015). "Ramp Tests: A Novel Approach to VIV Model Testing of Flexible Cylinders Using Continuously Varying Towing Speeds," *Int Conf Offshore Mech Arct Eng*, St John's, Canada, ASME, 2, V002T08A059. https://doi.org/10.1115/OMAE2015-42286.

Roveri, FE, and Vandiver, JK (2001). "SlenderEx: Using SHEAR7 for Assessment of Fatigue Damage Caused by Current Induced Vibrations," *Proc 20th Int Conf Offshore Mech Arct Eng*, Rio de Janeiro, Brazil, ASME, 3–8.

Rudy, S, Fan, D, del Aguila Ferrandis, J, Sapsis, TP, and Triantafyllou, MS (2022). "Optimized Parametric Hydrodynamic Databases Provide Accurate Response Predictions and Describe the Physics of Vortex-induced Vibrations," *J Fluids Struct*, 112, 103607. https://doi.org/10.1016/j.jfluidstructs.2022.103607.

Sarpkaya, T (1995). "Hydrodynamic Damping, Flow-induced Oscillations, and Biharmonic Response," *J Offshore Mech Arct Eng*, 117(4), 232–238. https://doi.org/10.1115/1.2827228.

Triantafyllou, M, Triantafyllou, G, Tein, YS, and Ambrose, BD (1999). "Pragmatic Riser VIV Analysis," *Proc Offshore Technol Conf*, Houston, TX, USA, Offshore Technology Conference, OTC-10931-MS. https://doi.org/10.4043/10931-MS.

Wang, XQ, So, RMC, and Chan, KT (2003). "A Non-linear Fluid Force Model for Vortex-induced Vibration of an Elastic Cylinder," *J Sound Vib*, 260(2), 287–305. https://doi.org/10.1016/S0022-460X(02)00945-8.

Wang, JS, Fan, D, and Lin, K (2020). "A Review on Flow-induced Vibration of Offshore Circular Cylinders," *J Hydrodyn*, 32(3), 415–440. https://doi.org/10.1007/s42241-020-0032-2.

Wang, Z, Fan, D, and Triantafyllou, MS (2021). "Illuminating the Complex Role of the Added Mass During Vortex Induced Vibration," *Phys Fluids*, 33(8), 085120. https://doi.org/10.1063/5.0059013.

Wang, Z, Fan, D, Triantafyllou, MS, and Karniadakis, GE (2021). "A Large-eddy Simulation Study on the Similarity Between Free Vibrations of a Flexible Cylinder and Forced Vibrations of a Rigid Cylinder," *J Fluids Struct*, 101, 103223. https://doi.org/10.1016/j.jfluidstructs.2021.103223.

Wang, Z, Li, A, et al. (2021). "Asymmetric Vortex Pair Induces Secondary Traveling Wave Vibration of a Flexible Cylinder from Still Water to Incoming Flow," *Phys Fluids*, 33(12), 125115. https://doi.org/10.1063/5.0075148.

Williamson, CH (1996). "Vortex Dynamics in the Cylinder Wake," *Annu Rev Fluid Mech*, 28(1), 477–539. https://doi.org/10.1146/annurev.fl.28.010196.002401.

Williamson, CH, and Govardhan, R (2004). "Vortex-induced Vibrations," *Annu Rev Fluid Mech*, 36, 413–455. https://doi.org/10.1146/annurev.fluid.36.050802.122128.

Williamson, CHK, and Govardhan, R (2008). "A Brief Review of Recent Results in Vortex-induced Vibrations," *J Wind Eng Ind Aerodyn*, 96(6–7), 713–735. https://doi.org/10.1016/j.jweia.2007.06.019.

Wu, B, Le Garrec, J, Fan, D, and Triantafyllou, MS (2017). "Kill Line Model Cross Flow Inline Coupled Vortex-induced Vibration," *Proc 36th Int Conf Offshore Mech Arct Eng*, Trondheim, Norway, ASME, 2, V002T08A010. https://doi.org/10.1115/OMAE2017-61191.

Wu, J, et al. (2020). "Improved VIV Response Prediction Using Adaptive Parameters and Data Clustering," *J Mar Sci Eng*, 8(2), 127. https://doi.org/10.3390/jmse8020127.

Wu, W, Bernitsas, MM, and Maki, K (2014). "RANS Simulation Versus Experiments of Flow Induced Motion of Circular Cylinder with Passive Turbulence Control at $35{,}000 < Re < 130{,}000$," *J Offshore Mech Arct Eng*, 136(4), 041802. https://doi.org/10.1115/1.4027895.

Wu, X, Ge, F, and Hong, Y (2012). "A Review of Recent Studies on Vortex-induced Vibrations of Long Slender Cylinders," *J Fluids Struct*, 28, 292–308. https://doi.org/10.1016/j.jfluidstructs.2011.11.010.

Xu, Y, Fu, S, Chen, Y, Zhong, Q, and Fan, D (2013). "Experimental Investigation on Vortex Induced Forces of Oscillating Cylinder at High Reynolds Number," *Ocean Systems Eng*, 3(3), 167–180. https://doi.org/10.12989/ose.2013.3.3.167.

Yin, D, et al. (2021). "Optimization of Hydrodynamic Coefficients for VIV Prediction," *Proc 40th Int Conf Offshore Mech Arct Eng*, virtual, online, ASME, 8, V008T08A025. https://doi.org/10.1115/OMAE2021-63890.

Zheng, H, Price, R, Modarres-Sadeghi, Y, Triantafyllou, GS, and Triantafyllou, MS (2011). "Vortex-induced Vibration Analysis (VIVA) Based on Hydrodynamic Databases," *Proc 2011 30th Int Conf Ocean Offshore Arct Eng*, Rotterdam, The Netherlands, ASME, 44397, 657–663. https://doi.org/10.1115/OMAE2011-50192.

APPENDIX A: HYDRODYNAMIC COEFFICIENT DATABASE PARAMETRIZATION

The mathematical formulation of the parametric reduced order model of the hydrodynamic coefficient database is as follows. According to Eq. 7, C_{my} is a function of f_r, and C_{lv} is a multivariable function of both f_r and A^*. Thus, to parametrize the latter, intermediate curves are introduced. Before proceeding to the coefficient formulation, the softplus function should be defined:

$$sf(x, \boldsymbol{p}) = p_{19} \cdot \ln\left(1 + \exp\frac{x}{p_{19}}\right) \tag{A1}$$

where p_{19} serves as a scaling constant. Then, the C_{my} curve may be parametrized as follows.

$$\begin{aligned} C_{my}(f_r, \boldsymbol{p}) = p_{15} &+ \frac{p_{16} - p_{15}}{p_6 - p_2}[sf(f_r - p_2) - sf(f_r - p_6)] \\ &+ \frac{1 - p_{16}}{p_8 - p_7}[sf(f_r - p_7) - sf(f_r - p_8)] \end{aligned} \tag{A2}$$

$C_{lv,0}$ may be represented parametrically, as shown below.

$$\begin{aligned} C_{lv,0}(f_r, \boldsymbol{p}) = &\frac{p_9}{p_2 - p_1}[sf(f_r - p_1) - sf(f_r - p_2)] \\ &+ \frac{p_{10} - p_9}{p_3 - p_2}[sf(f_r - p_2) - sf(f_r - p_3)] \\ &+ \frac{p_{11} - p_{10}}{p_4 - p_3}[sf(f_r - p_3) - sf(f_r - p_4)] \\ &+ \frac{-p_{11}}{p_5 - p_4}[sf(f_r - p_4) - sf(f_r - p_5)] \end{aligned} \tag{A3}$$

The A_c^* curve may be represented as follows.

$$\begin{aligned} A_c^*(f_r, \boldsymbol{p}) = &\frac{p_{12}}{p_2 - p_1}[sf(f_r - p_1) - sf(f_r - p_2)] \\ &+ \frac{p_{13} - p_{12}}{p_3 - p_2}[sf(f_r - p_2) - sf(f_r - p_3)] \\ &+ \frac{p_{14} - p_{13}}{p_4 - p_3}[sf(f_r - p_3) - sf(f_r - p_4)] \\ &+ \frac{-p_{14}}{p_5 - p_4}[sf(f_r - p_4) - sf(f_r - p_5)] \end{aligned} \tag{A4}$$

Finally, the lift coefficient, C_{lv} may be calculated as follows.

$$C_{lv}(A^*, \boldsymbol{p}) = \begin{cases} C_{lv,0} + p_{17} \cdot A^* & \text{if } A^* \le A_c^* \\ C_{lv,0} + p_{17} \cdot A_c^* - p_{18} \cdot (A^* - A_c^*) & \text{if } A^* > A_c^* \end{cases} \tag{A5}$$

The complete model of the parametric hydrodynamic coefficient database may be represented using four plots, one for each parametrized curve (i.e., C_{my} versus f_r, $C_{lv,0}$ versus f_r, A_c^* versus f_r, and C_{lv} versus A^*, as shown in Fig. A.1 (in that order, from left to right).

As Fig. A.1 illustrates, the model parametrized the curves as piecewise linear functions, which are smoothed using a softplus function. The parametrization allows flexibility in terms of magnitudes and transition points between linear sections. It should be noted that some parameters are shared between the curves to restrict the model's dimensionality.

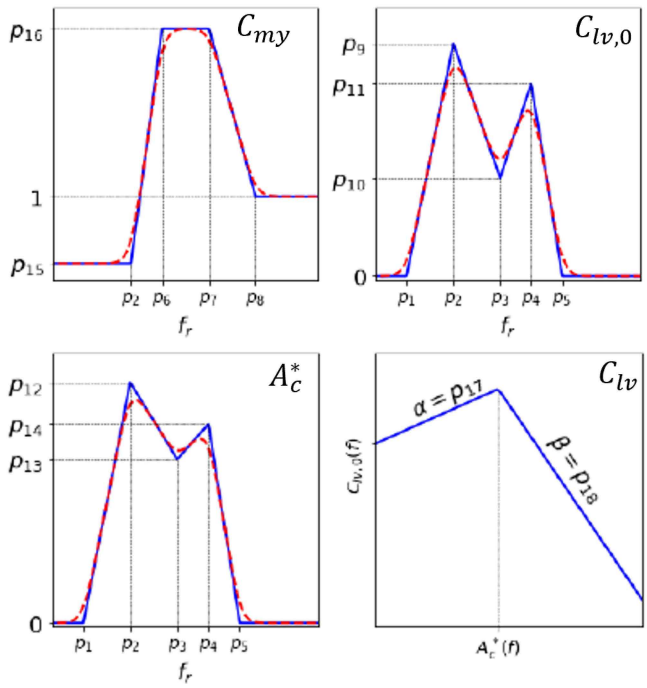

Fig. A.1 Hydrodynamic coefficient database parametrization, as shown from left to right: C_{my} versus f_r, $C_{lv,0}$ versus f_r, A_c^* versus f_r, and C_{lv} versus A^*. Nineteen parameters are used to parametrize the hydrodynamic coefficient database in a reduced order model fashion. The parameters serve as the hydrodynamic features that are learned from experimental data. The learned parameters with the forward model constitute a data-informed framework used to predict flexible riser VIV.

APPENDIX B: DATA SPECIFICATIONS

Catenary Riser in Uniform Flow

The data used for the catenary riser in uniform flow results were collected as part of the NDP by Lie (2001). The report was published by MARINTEK (Trondheim, Norway). The experiment numbers and corresponding flow velocities for the incidence angle of 0 degrees between the catenary plane and the flow are shown in Table B.1. The experiment numbers and corresponding flow velocities for the incidence angle of 30 degrees between the catenary plane and the flow are shown in Table B.2.

Test number	Flow speed	Test number	Flow speed	Test number	Flow speed
1000	0.12	1008	0.20	1016	0.28
1002	0.14	1010	0.22	1018	0.30
1004	0.16	1012	0.24	1020	0.32
1006	0.18	1014	0.26	1022	0.34

Table B.1 NDP SCR: Incidence angle of 0 degrees

Test number	Flow speed	Test number	Flow speed	Test number	Flow speed
2004	0.12	2008	0.20	2016	0.28
2001	0.14	2010	0.22	2018	0.30
2002	0.16	2012	0.24	2020	0.32
2006	0.18	2014	0.26	2022	0.34

Table B.2 NDP SCR: Incidence angle of 30 degrees

Vertical Riser in Uniform Flow

The data used for the vertical riser in uniform flow results were collected as part of the NDP by Braaten and Lie (2004). The report was published by MARINTEK.

A vertical riser model with length over diameter ratio $L/D \approx$ 1,400 was towed at Reynolds numbers $Re_D \approx 7.1 \cdot 10^3$ to $5.7 \cdot 10^4$. Tested velocities were in the range of 0.3 to 2.4 m/s. The experiment numbers and corresponding flow velocities are shown in Table B.3.

Test no.	Flow velocity	Test no.	Flow velocity	Test no.	Flow velocity	Test no.	Flow velocity
2010	0.3	2070	0.9	2130	1.5	2191	2.1
2020	0.4	2080	1.0	2141	1.6	2201	2.2
2030	0.5	2090	1.1	2150	1.7	2210	2.3
2040	0.6	2100	1.2	2160	1.8	2220	2.4
2050	0.7	2110	1.3	2170	1.9		
2060	0.8	2120	1.4	2182	2.0		

Table B.3 NDP vertical riser